ANALYSIS OF AVIRIS DATA: A COMPARISON OF THE PERFORMANCE OF COMMERCIAL SOFTWARE WITH PUBLISHED ALGORITHMS

William H. Farrand[1]

1. Introduction

An early handicap to the effective use of AVIRIS data was a lack of appropriate software (Vane and Goetz, 1993). With improvements to the AVIRIS sensor have also come improvements in the available software. While there are a variety of software packages currently in use, a review of the recent literature indicates that most users of AVIRIS data are using the commercial ENVI software. The documentation provided with the ENVI software (RSI, 2000) is generally quite adequate; however, specifics on how most processing routines are implemented are not provided. Moreover, the source code for ENVI routines are not readily available, thus the user who is curious about how certain algorithms are implemented is left with few options. The objective of this paper is to provide a comparison of how ENVI implementations of several mapping algorithms perform against implementations of those routines coded by the author from the original published algorithms. The mapping algorithms examined in this work are: linear spectral mixture analysis, constrained energy minimization/matched filtering, and band mapping. The ENVI routines used were from ENVI version 3.4 software release.

2. Spectral Mixture Analysis

While the ENVI User's Guide provides several references for linear spectral mixture analysis, the author compared results obtained from the ENVI "Linear Spectral Unmixing" module with those obtained from the algorithm developed at the University of Washington and described by Adams et al. (1993) and in earlier papers such as Smith et al. (1990), Possollo et al. (unpublished manuscript), and Gillespie et al. (1990). This algorithm will henceforth be referred to as the "UW algorithm."

The basis of linear spectral unmixing is to model the response of each spatial element as a linear combination of endmember spectra. The basis equation for linear spectral mixture analysis (SMA) is:

$$r(x,y) = \alpha\mathbf{M} + n$$

where: $r(x,y)$ = the relative reflectance spectrum for the pixel at position (x,y)
α = the vector of endmember abundances
$\mathbf{M}$ = the matrix of endmember spectra
n = the vector of residuals between the modeled and the measured reflectances

The result of Spectral Mixture Analysis (SMA) is a series of "fraction images" for each endmember wherein the data numbers range, ideally, between 0 and 1. Fraction image pixels with a DN of 0 are taken to be devoid of the endmember material. Fraction image pixels with a DN of 1.0 are taken to be completely covered with the endmember material.

The implementation of SMA in ENVI appears to be a relatively straightforward implementation that uses Singular Value Decompositon (SVD) to determine endmember abundances as detailed in Boardman (1989). The implementation of SMA described in the earlier references is slightly different in the way that it treats a "shade" endmember. The shade endmember is not a physical material but rather represents the "dark point" in the image scene; i.e., an ideal shade endmember would be a shadowed surface with zero reflectance at all wavelengths. While shade is not necessary for all analyses in which SMA can be used, it can be quite helpful for use in areas with substantial topographic relief, for use with forested scenes (to help determine canopy shade), or as a measure of surface roughness. Also, the procedure described in the ENVI User's Guide (RSI, 2000) for determining image endmembers almost always leads to the selection of a dark point image endmember. This ENVI method for

[1] Farr View Consulting/Space Science Institute, Boulder, Colorado (farrand@colorado.edu)

A. 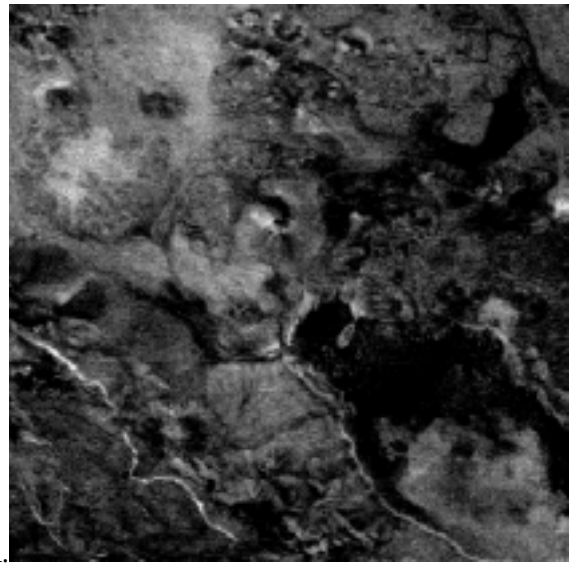 B. 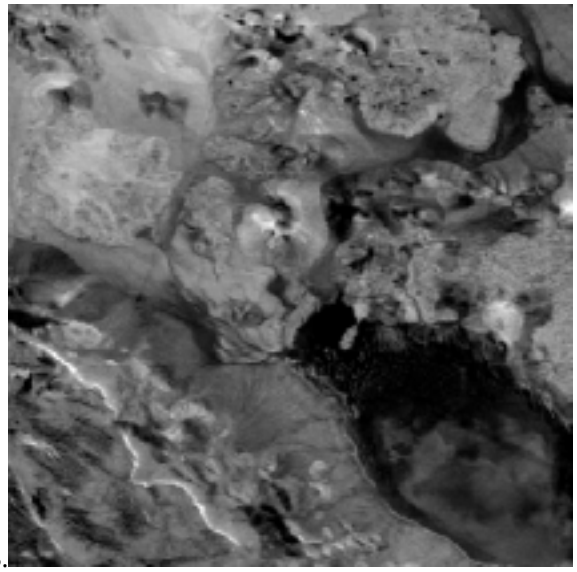

Figure 1. Comparison of shade images for AVIRIS scene over Lunar Crater Volcanic Field, Nevada, derived from applying SMA as implemented in A. ENVI and B. UW algorithm. Fraction images have been stretched between 0 and 1. The prominent diagonal cutting across the lower left corner represents shadows cast by a major cliff face.

determining image endmembers (eg., Boardman and Kruse, 1994) starts with the use of a Minimum Noise Fraction (MNF) transform to reduce spectral dimensionality. This is followed by the Pixel Purity Index reduction to find "spectrally pure" pixels. Finally, the ENVI n-dimensional visualization tool is used to find extreme "vertex" pixels at the edges of the n-dimensional data cloud. As mentioned above, in this author's experience if there is any significant shadowing in the scene, these "dark point" pixels will cluster together and generally constitute one of the more prominent clusters in the n-D data cloud. The user who selects these "shade" pixels might want to use them as an endmember in SMA. Thus, it is appropriate to determine how well the ENVI implementation of SMA treats shade.

The way that shade is handled in the UW algorithm is that:

1. the shade endmember spectrum is first subtracted from all other endmember spectra (eg., the "material" endmembers),
2. the endmember matrix is inverted to derive endmember fractions[2],
3. the sum of the material fraction images is subtracted from 1.0 and this difference is taken to be the shade fraction image.

The analyst who includes shade as an endmember with the ENVI "Linear Spectral Unmixing" module is including shade as a material endmember. Given the low data values in the shade endmember spectrum, erroneous fraction images can potentially result. Figure 1 shows shade fraction images derived from a 1994 AVIRIS scene of the Lunar Crater Volcanic Field in Nye County, Nevada. There are few if any substantive differences between the two fraction images. Shadowed to dark areas are bright as is expected. DN values of both fraction images are generally between 0 and 1.0 for both. This result ran counter to expectations since the author has observed flaws in shade fraction images derived from using the ENVI SMA implementation in past work. Specifically, when applied to lower dimensionality, multispectral data erroneous shade fraction images can result. An example is provide in Figure 2 wherein the same AVIRIS scene has been spectrally resampled to match the spectral bandpasses of the nine visible through SWIR channels of the ASTER sensor (Abrams, 2000). In this case, there is a marked difference between the two shade fraction images with the one derived from ENVI having erroneous shade fractions. The actual data values for the ENVI derived shade fraction image shown in Fig. 2a are all negative while those for the

[2] Possollo et al. (unpublished manuscript) describe the matrix inversion algorithm used in the UW implementation as being the QR factorization rather than SVD.

A. 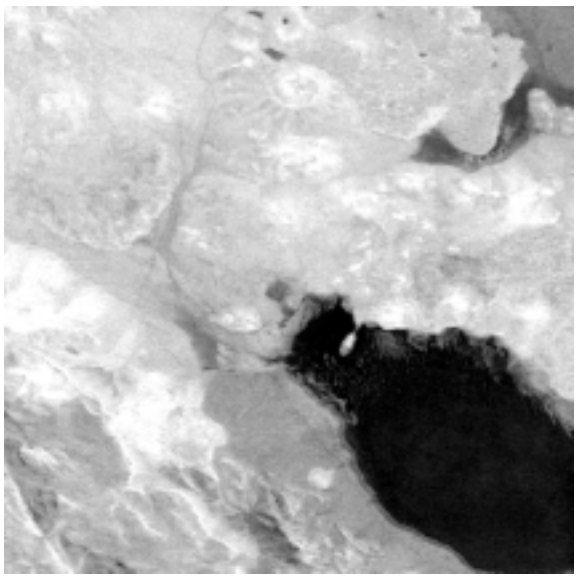 B. 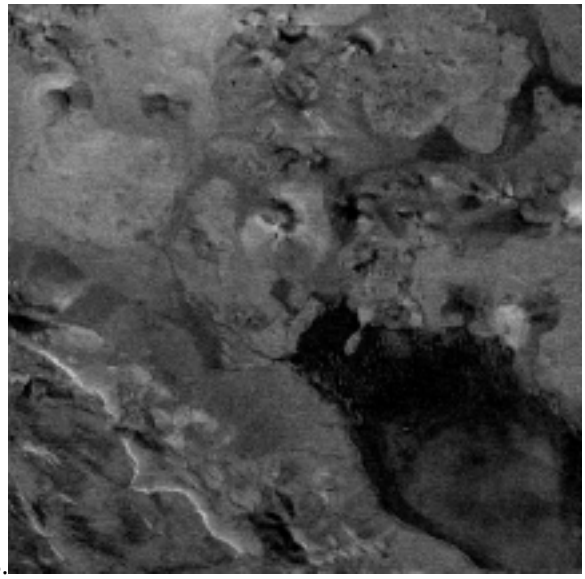

Figure 2. AVIRIS scene from Fig. 1 was resampled to ASTER Visible-SWIR bandpasses and SMA was applied. A. ENVI derived shade fraction image B. Shade fraction image derived from application of UW algorithm.

shade fraction image derived from the UW algorithm are predominantly between 0 and 1.0 as is desired for a fraction image.

While the straightforward linear spectral unmixing algorithm of ENVI does not handle shade in the same manner as the UW algorithm, the procedures implemented in the latter algorithm can be carried out entirely in ENVI. The ENVI "spectral math" routine can be used to subtract the shade endmember from the material endmembers. The ENVI linear spectral unmixing routine can be run using just the material endmembers. Then, using ENVI's "band math" routine, the sum of the material endmembers can be subtracted from 1.0 to produce a shade fraction image.

3. Constrained Energy Minimization/Matched Filter

ENVI has an implementation of a routine under the name of "Matched Filter" (MF) which is essentially the same algorithm described by Harsanyi (1993) and Farrand and Harsanyi (1997) as "Constrained Energy Minimization" (CEM). The CEM method is based on the linearly constrained adaptive beam-forming problem from the signal processing community. The solution to this problem is to minimize the average power received by a multielement antenna array subject to the constraint that a constant, unity response in the presumed direction of the target signal is maintained. In the instance of CEM/MF, a vector operator $\boldsymbol{w}$ is determined that suppresses the unknown and undesired background spectra while enhancing that of the known target spectrum, $\boldsymbol{d}$. The operator, $\boldsymbol{w}$, is defined by constraints to minimize the total output energy of all pixels and to require that when the operator is applied to the target signature, the output is 1.0. A solution that meets these constraints is provided by:

$$\boldsymbol{w} = \frac{\mathbf{R}_r^{-1}\boldsymbol{d}}{\boldsymbol{d}^T\mathbf{R}_r^{-1}\boldsymbol{d}}$$

where: $\mathbf{R}_r^{-1}$ = the inverse of the sample correlation matrix of the hyperspectral scene. Since $\mathbf{R}$ is ill-conditioned for hyperspectral images, it is difficult to calculate $\mathbf{R}^{-1}$. To circumvent this difficulty, the sample correlation matrix can be approximated by:

$$\mathbf{R} = \mathbf{V}\Lambda\mathbf{V}^T$$

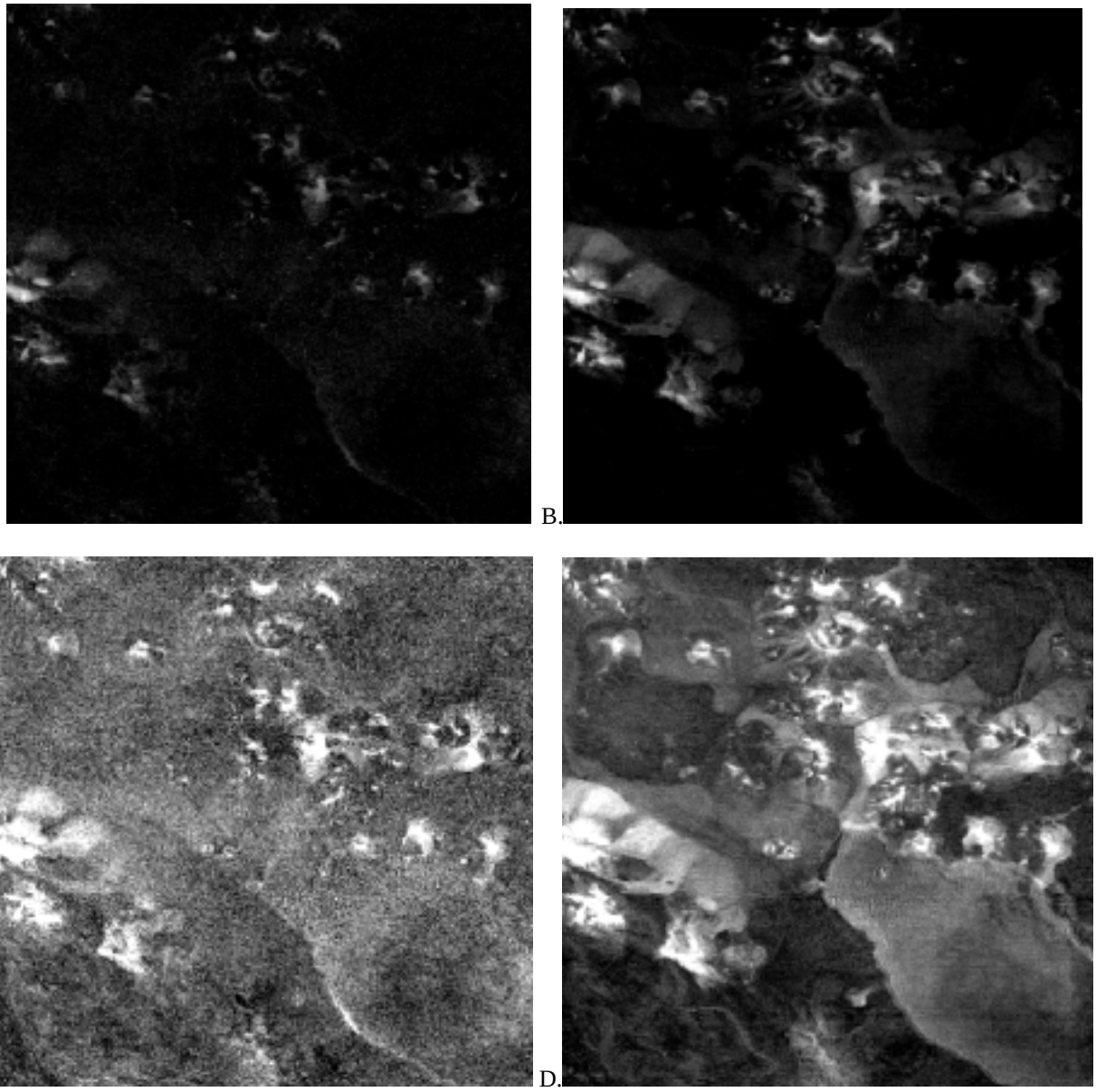

Figure 3: A. ENVI Matched Filter fraction image of red cinders for Lunar Crater Volcanic Field AVIRIS scene. Contrast stretch 0 to 1.0. B. CEM fraction image of red cinders for same scene with contrast stretch from 0 to 1.0. C. Same image as A. with no stretch. D. Same image as B. with no stretch.

where: **V** is a matrix populated by the eigenvectors of the sample correlation matrix, and Λ is a diagonal matrix with the eigenvalues of the sample correlation matrix. **V** can be approximated by a smaller matrix populated just with the first *p* significant eigenvectors. How to determine the value of *p* (i.e., how many significant eigenvectors are there?) can be somewhat subjective and in the author's experience the best results have been achieved by sometimes running CEM several times using a different number of significant eigenvectors each time. Unfortunately, the ENVI implementation of Matched Filter does not allow the user to specify the number of principal eigenvectors that will be used. Boardman (personal communication) suggests that this becomes a non-issue if MF is run not against the original AVIRIS data (or AVIRIS data converted to reflectance as was done in this study), but against the MNF-transformed data. However, this approach is not mentioned in the ENVI User's Guide; thus, the author compared results obtained from CEM, using a personally determined optimum number of principal eigenvectors, with those obtained running the ENVI MF routine against a non-MNF transformed AVIRIS scene. Figure 3 shows fraction images obtained from ENVI MF and from CEM for a red cinder target signature on the

same LCVF AVIRIS scene used above. Although the results are different, both are acceptable fraction images of the cinders; however, the unstretched versions of the images show a higher response from background materials in the MF image than in the CEM image- indicating a sub-optimal suppression of those background signatures.

Given that routines such as MF are often used for mineral exploration, a trial was also conducted using 1998 AVIRIS data collected over the Tushar Mountains/Marysvale mining district in central Utah (Farrand, 2000; Rockwell et al., 2000). In the author's experience, when mapping minerals whose diagnostic spectral features are in the SWIR (eg., alunite, kaolinite, etc.), the best results are obtained using a subset of SWIR channels. Likewise, when mapping Fe^{3+} - bearing minerals such as hematite and goethite, the best results are obtained using a VNIR only subset. This approach was pursued in this trial. Also, in this instance since the AVIRIS data were of high quality and there were excellent exposures of the target minerals, library spectra (from the USGS spectral library, Clark et al., 1993) were convolved to AVIRIS bandpasses and used as the target spectra. The results are shown in Figure 4 for a trial with kaolinite and in Figure 5 for a trial with hematite. It can be seen that the CEM and MF results for kaolinite are nearly identical while those for hematite show, as in the LCVF example above, a relatively high response from background materials for the MF versus the CEM image. The better performance of MF in the SWIR is attributed to a better ability to detect the proper cut-off point for the number of principal eigenvectors used in the suppression of the undesired background. There are more complicating background materials (primarily vegetation) with responses in the VNIR which make the selection of a proper number of principle eigenvectors more of a challenge for that spectral range.

4. Spectral Feature Fitting

Clark et al. (1990) described the algorithm that was the basis of what would evolve into the current USGS Tetracorder algorithm (Clark, 2001). While the current version of Tetracorder is a complex expert system, the basis algorithm is relatively simple. The "band mapping algorithm" described by Clark et al. (1990) is briefly recapitulated below. To map a given mineral with a specific absorption feature, for example, the 2.21 μm kaolinite doublet, a high resolution laboratory spectrum is re-sampled to the spectral resolution of AVIRIS. The spectrum is sub-sampled to match the specific absorption feature (i.e., only bands from the short wavelength shoulder of the absorption to the long wavelength shoulder are included). A straight line continuum (calculated based on a line between the two band shoulders) is divided out from both the laboratory and the AVIRIS spectra. The contrast between the library and the AVIRIS spectra are mitigated through the use of an additive constant, *k*. This constant is incorporated into a set of equations which are solved through the use of standard least squares.

A. 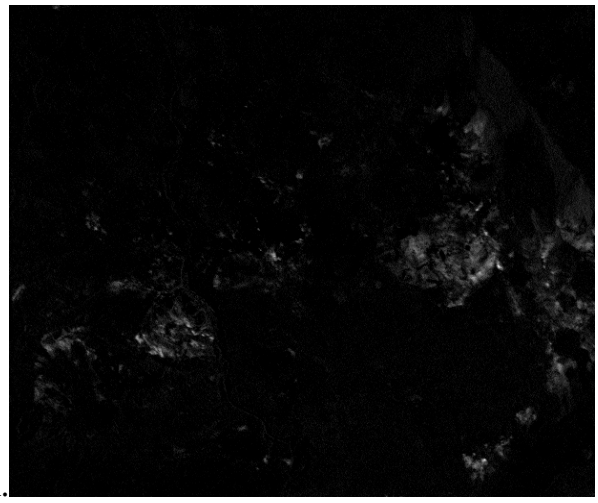 B. 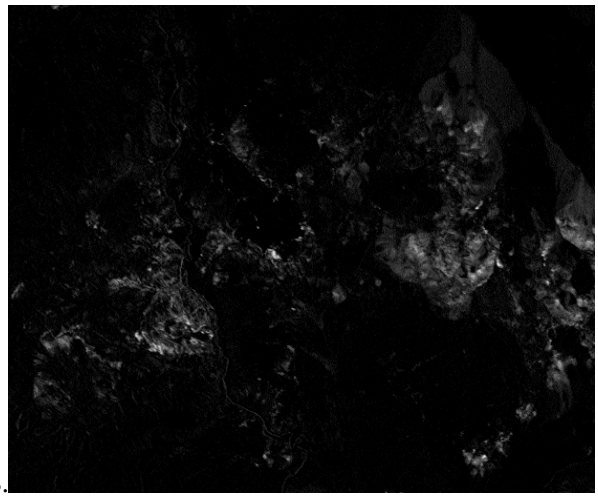

Figure 4. Comparison of fraction images derived for a library kaolinite target signature over the eastern Tushar Mountains/Marysvale mining district using A. ENVI Matched Filter (MF), and B. Constrained Energy Minimization (CEM). Images have been stretched between 0 and 1.

A. 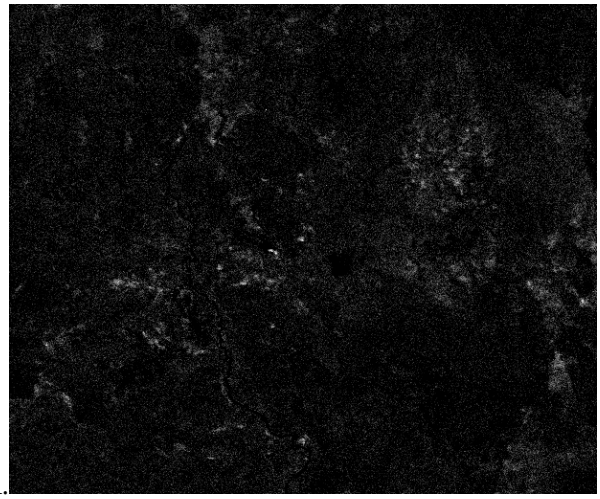 B. 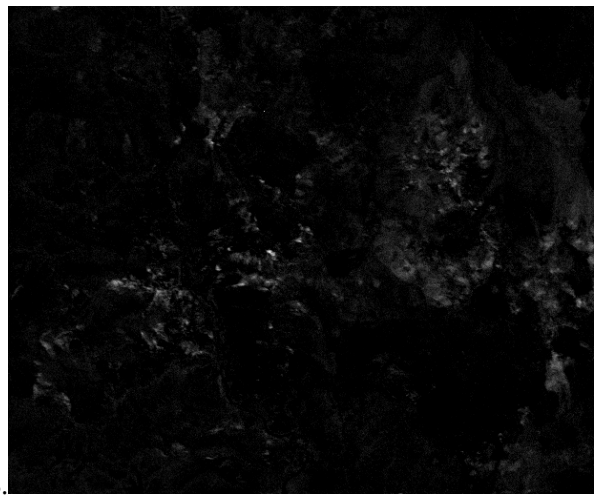

Figure 5. Comparison of fraction images derived for a library hematite target signature over the eastern Tushar Mountains/Marysvale mining district using A. ENVI Matched Filter (MF), and B. Constrained Energy Minimization (CEM). Images have been stretched between 0 and 1.

The result of the Clark et al. (1990) band mapping algorithm are two data numbers per spatial sample of the AVIRIS scene. First the band depth of the feature is calculated, and second a goodness-of-fit parameter is calculated. These two parameters are most often combined in a band depth times goodness-of-fit image.

The "Spectral Feature Fitting" routine incorporated in ENVI presumably uses similar equations to those recounted by Clark et al. (1990), but the basis equations for the ENVI algorithm are not provided in the ENVI User's Guide. Indeed, the output from the ENVI algorithm is rather different from that of the USGS band mapping algorithm. The output consists of a "scale" image, which appears comparable to the band depth image output by the band mapping algorithm, and a root mean square (rms) error image is also output. Presumably, the latter is the actual rms error of the fit between the library and the AVIRIS spectrum. The two images can be combined by dividing the scale image by the rms error image.

The author coded the band mapping algorithm described by the Clark et al. (1990) paper and compared results with those obtained by ENVI for the AVIRIS scene covering the eastern Tushar Mountains and Marysvale mining district in central Utah. Maps were produced of kaolinite, illite, and alunite. There were no substantive differences between the band depth times goodness-of-fit images derived from the band mapping algorithm and the scale/rms error images derived from the ENVI "spectral feature fitting" routine.

5. Conclusions

This study presented a comparison of the results obtained from implementations of published algorithms coded by the author and ENVI implementations of the corresponding algorithms. The linear spectral unmixing algorithm implemented in ENVI handles a "dark point" or "shade" endmember differently than the published Adams et al. (1993) spectral mixture analysis algorithm (SMA). It was found that using high dimensionality AVIRIS data, the dark point endmember could still be used to produce a reasonable fraction image; however, using lower dimensionality simulated multispectral data, the ENVI implementation of SMA produced an unreasonable "shade" fraction image.

In a comparison of Constrained Energy Minimization (Harsanyi, 1993; Farrand and Harsanyi, 1997) versus the ENVI implementation of the equivalent Matched Filter algorithm, it was found that results were generally similar; however, for materials whose primary spectral expression lie in the VNIR, the ENVI MF routine provided a sub-optimal suppression of the background. However, the performance of the MF routine can supposedly be enhanced by using it against MNF-transformed data (Boardman, personal communication).

It was found that results from the ENVI "spectral feature fitting" routine were essentially the same as those obtained from the Clark et al. (1990) band mapping algorithm. In using either approach, the analyst must exercise

care to use only those channels covering the absorption band of interest. In an early trial, the author used most of the AVIRIS spectrometer D channels with the ENVI "spectral feature fitting" algorithm and the results were inaccurate compared to those obtained in later trials using more precise spectral subsections covering just the absorption features of interest.

6. References

Abrams, M., 2000, "The Advanced Spaceborne Thermal Emission and Reflection Radiometer (ASTER): Data products for the high spatial resolution imager on NASA's Terra platform". *Int. J. Remote Sensing*, vol. 43, no. 5, pp. 847-859.

Adams, J.B., M.O. Smith, and A.R. Gillespie, 1993, "Imaging spectroscopy: Interpretation based on spectral mixture analysis". In *Remote Geochemical Analysis: Elemental and Mineralogical Composition*, edited by C.M. Pieters and P.A.J. Englert (New York: Cambridge University Press), pp. 145-166.

Boardman, J.W., 1989, "Inversion of imaging spectrometry data using singular value decomposition", in *Proc. IGARSS '89, 12th Canadian Symposium on Remote Sensing*, vol. 4, pp. 2069-2072.

Boardman, J.W., and F.A. Kruse, 1994, "Automated spectral analysis: A geological example using AVIRIS data, north Grapevine Mountains, Nevada", in *Proc. ERIM Tenth Thematic Conf. on Geologic Remote Sensing*, pp. I-407 – I-418.

Clark, R.N., 2001, "Tetracorder description and demonstration", Proc. 9th JPL Airborne Earth Science Workshop, (in press).

Clark, R.N., G.A. Swayze, A.J. Gallagher, T.V.V. King, and W.M. Calvin, 1993, "The U.S.G.S. Digital Spectral Library: Version 1: 0.2 to 3.0 μm". U.S. Geol. Surv. Open File Report 93-592.

Clark, R.N., A.J. Gallagher, and G.A. Swayze, 1990, "Material absorption band depth mapping of imaging spectrometer data using a complete band shape least-squares fit with library reference spectra," in *Proc. 2nd AVIRIS Workshop*, (R.O. Green, Ed.), JPL Publication 90-54, Pasadena, CA, pp. 176-186.

Farrand, W.H., 2000, "Mapping alteration mineralogy in the Tushar Mountains and Marysvale mining district, Utah using AVIRIS data". *Proceedings of the Fourteenth International Conference on Applied Geologic Remote Sensing*, pp. 62-69.

Farrand, W.H. and J.C. Harsanyi, 1997, "Mapping the distribution of mine tailings in the Coeur d'Alene River Valley, Idaho through the use of a Constrained Energy Minimization technique." *Remote Sens. Env.* vol. 59, pp. 64-76.

Gillespie, A.R., M.O. Smith, J.B. Adams, S.C. Willis, A.F. Fischer III, and D.E. Sabol, 1990, "Interpretation of residual images: Spectral mixture analysis of AVIRIS images, Owens Valley, California," in *Proc. 2nd AVIRIS Workshop*, (R.O. Green, Ed.), JPL Publication 90-54, Pasadena, CA, pp. 243-270.

Harsanyi, J.C., 1993, "Detection and classification of subpixel spectral signatures in hyperspectral image sequences", PhD thesis, Univ. of Maryland Baltimore County, 116 pp.

Rockwell, B.W., et al., 2000, "Mineral mapping in the Marysvale Volcanic Field, Utah, using AVIRIS data", in Proc. 9th JPL Airborne Earth Science Workshop, (R.O. Green, Ed.), JPL Publication 00-18, Pasadena, CA, pp. 407-417.

Research Systems, Inc., 2000, ENVI 3.4 User's Guide.

Smith, M.O., S.L. Ustin, J.B. Adams, and A.R. Gillespie, 1990, "Vegetation in deserts: 1. A regional measure of abundance from multispectral images". *Remote Sens. Env.* vol. 31, pp. 1-26.

Vane, G. and A.F.H. Goetz, 1993, "Terrestrial imaging spectrometry: Current status, future trends", *Remote Sens. Env.*, vol. 44, pp. 117-126.